# Magnetism in $Co_{80-x}Fe_xB_{20}$: Effect of crystallization

R. Lavrijsen,[1,a)] P. V. Paluskar,[1] C. T. J. Loermans,[1] P. A. van Kruisbergen,[1] J. T. Kohlhepp,[1] H. J. M. Swagten,[1] B. Koopmans,[1] and E. Snoeck[2]
[1]*Department of Applied Physics, Center for NanoMaterials and COBRA Research Institute, Eindhoven University of Technology, P.O. Box 513, 5600 MB Eindhoven, The Netherlands*
[2]*CEMES-CNRS, 29 Rue Jeanne Marvig, B.P. 94347, F-31055 Toulouse Cedex 4, France*

(Received 24 November 2010; accepted 21 February 2011; published online 3 May 2011)

We report on the change in the structural and magnetic properties of magnetically soft ternary $Co_{80-x}Fe_xB_{20}$ alloys as a function of composition, thickness, and annealing temperature. Compositions high in cobalt show a significant change in coercivity after annealing. This is explained using the random anisotropy model by relating the magnetic exchange length to the grain size of the crystallites. The presented results are a systematic study explaining trends seen in the transition from soft to hard magnetic behavior, providing insight into why the soft CoFeB alloys have been so successful recently in spintronic devices. © *2011 American Institute of Physics*. [doi:10.1063/1.3575318]

## I. INTRODUCTION

Amorphous ferromagnetism in transition metal–borides (TM-B) has been extensively studied, mainly due to the magnetism observed in these materials and to their potential industrial applications.[1] The demonstration of record-high room temperature tunnel magnetoresistance (TMR) in CoFeB/$AlO_x$-based (Ref. 2) and CoFeB/MgO-based (Refs. 3–5) magnetic tunnel junctions (MTJs) has renewed the interest in the ferromagnetism exhibited by these alloys. Furthermore, they have been used to observe the spin-torque diode effect,[6] create perpendicular MTJs,[7] and facilitate record-low switching currents in spin-torque based MTJs.[8] Indeed, spawned by the search for novel materials to advance the performance of spintronic devices, these experimental results emphasize the superior electronic and transport properties of these amorphous ferromagnets and underscore their excellent potential for industrial applications.[1,9] Due to their amorphous/nanocrystalline nature, these alloys exhibit relatively small random anisotropy,[1,10] making them magnetically soft and suitable for the free layer in MTJs. In addition, being amorphous, they are highly insensitive to the miscibility of their constituents, allowing their compositions to be tuned to tailor their magnetic and electronic properties depending on the application.[11] Furthermore, they have Curie temperatures well above room temperature and exhibit low crystallization temperatures, providing an additional parameter for exploring their fundamental properties depending on their morphology.

Indeed, from the spintronics point of view, there have been extensive studies on the behavior of the TMR as a function of CoFeB composition and annealing temperature.[12–14] These studies focus on the post-annealing crystalline structure of CoFeB at the interface with the MgO tunnel barrier. The crystallization is known to induce a strong (100) texture of the MgO barrier, consequently leading to high TMR ratios in such annealed tunnel junctions. However, the annealing induced crystallization of CoFeB has an impact on the magnetic properties of nanothin CoFeB films as well. Moreover, this postannealing change in the magnetic properties may be expected to depend on the composition of the ternary amorphous alloy. A systematic study of the influence on the magnetic properties as well as the sensitivity to the alloy composition has not yet been performed in detail.

In this paper, we explore the correlation between the structural and magnetic properties of CoFeB alloys induced by an annealing treatment depending on the thickness and the composition of the $Co_{80-x}Fe_xB_{20}$ alloys. The CoFeB in this study is grown on and capped with thin Al layers; therefore we concentrate on the crystallization of CoFeB when grown on and capped with Al. This is a different case than in the aforementioned studies, in which the CoFeB is grown on MgO. We, however, are convinced that our observations and interpretation relating the magnetic behavior to the morphology and intrinsic properties of the different CoFeB compositions are of relevance for the MgO studies as well. We find that annealing has a remarkable effect on the coercivity ($H_c$) of nanothin layers, which shows a dramatic increase depending not only on the annealing temperature but also on the thickness of the layer. We explain the observed trends in the coercivity by using the random anisotropy model,[15] which relates the magnetic exchange length ($L_{ex}$) to the crystallite grain size ($D$). The results open up a way to tune the grain size $D$ and $H_c$ in CoFeB films by choosing a certain thickness ($t$) and annealing temperature ($T_a$). Finally, this study gives a hint as to why the magnetically soft CoFeB films are so successfully used in applications, and it will provide handles to further exploit their potential.

The paper is organized as follows: We start with the experimental details in Sec. II. This is followed by an x-ray diffraction (XRD) study in Sec. III, where direct proof of the crystallization of the CoFeB layers after an annealing treatment is presented. Then we concentrate on the effect of the crystallization on the magnetic properties in Sec. IV, where, for clarity, we explain the observed trends using a single

[a)]Author to whom correspondence should be addressed. Electronic mail: r.lavrijsen@tue.nl.

 

composition. To correlate the local morphology of the crystallized films with the magnetic properties, we present a high-resolution cross-section transmission electron microscopy (HRTEM) analysis in Sec. V. The HRTEM analysis allows us to introduce a model in Sec. VI that can be used to describe the observed trends in the coercivity. This is followed by an exploration of the effect of the annealing temperature on the magnetic properties in Sec. VII. Finally, we present a possible explanation of the difference in the magnetic properties after annealing when the composition of the CoFeB is varied. We conclude the paper with a short summary of the main conclusions and give some final remarks.

## II. EXPERIMENTAL DETAILS

The samples under investigation are Si/$SiO_x$/Al (3.5 nm)/$Co_{80-x}Fe_xB_{20}$ (70 nm)/Al (3.5 nm), with $x$ (in at.%) ranging from 8% to 72% in steps of 12%. They were prepared by dc magnetron sputtering (base pressure $< 10^{-8}$ mbar) at room temperature. We investigated their structural properties using high-angle XRD (Cu $K_\alpha$) and HRTEM. The magneto-optical Kerr effect (MOKE) was used to investigate the magnetic properties. We deposited wedge-shaped samples to investigate the magnetic properties as a function of the CoFeB layer thickness $t$, which varied from 0 to 70 nm over a length of 15 mm. The wedge was scanned using a MOKE laser spot with a diameter of 75 $\mu$m to locally probe the magnetic properties. This was done for as-deposited samples and after annealing at $T_a = 200$ to 490 °C for 30 min in an Ar environment with a magnetic field of 250 kA/m.

## III. XRD ON $Co_{80-x}Fe_xB_{20}$

In Fig. 1, the XRD intensity pattern for as-deposited and annealed ($T_a = 450$ °C) samples is shown for the region of interest, where diffraction peaks are known to appear for crystallized $Co_{80-x}Fe_xB_{20}$.[16–19] We have chosen to limit our XRD analysis to relatively thick films of $t = 70$ nm to obtain a sufficient signal to noise ratio. In the as-deposited case, as expected for an amorphous film, we do not observe any diffraction peaks other than from the Si substrate over a large range of diffraction angles (a representative measurement for $x = 80$ is shown). Diffraction peaks start to appear in the spectrum for $T_a > 300$ °C (not shown), indicating the onset of the crystallization process, consistent with the literature.[17] For $T_a = 450$ °C, the observed diffraction peaks for $Co_{80-x}Fe_xB_{20}$ are rather broad. Based on several studies, the morphology of the annealed films can be imagined as polycrystalline with a large spread in grain size $D$ embedded in an amorphous matrix.[12,13,18] Evidently, the varying peak position indicates that the lattice constant for the crystallized films changes with the composition of the film. Plotting the lattice constant of the crystallized films as a function of the Fe content (see inset in Fig. 1) reveals the well-known Slater–Pauling behavior of the lattice constant as seen earlier.[20] Now that we have seen that the annealing treatment induces crystallization of the CoFeB layer, we turn to the effect of the crystallization on the magnetic behavior.

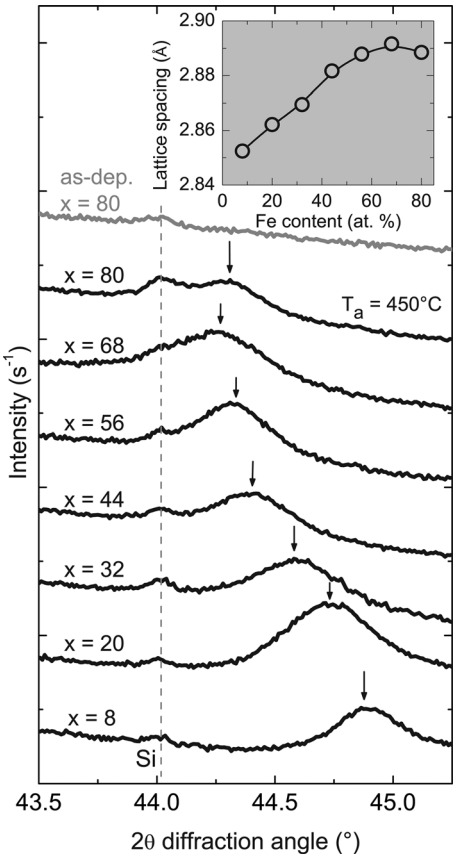


FIG. 1. XRD measurements of $Co_{80-x}Fe_xB_{20}$ films annealed at $T_a = 450$ °C. A representative measurement for the as-deposited case of $x = 80$ is shown in gray. The inset shows the lattice constant, comparable to the measurements of Ellis *et al.* (Ref. 20).

## IV. TRANSITION FROM SOFT TO HARD MAGNETISM

To investigate the impact of the crystallization of the $Co_{80-x}Fe_xB_{20}$ films on their magnetic properties, to begin with, we investigated the behavior of the coercivity of a single CoFeB composition as a function of film thickness before and after annealing at $T_a = 450$ °C. Figure 2(a) shows MOKE measurements of a wedge-shaped $Co_{60}Fe_{20}B_{20}$ sample with $t = 0$ to 70 nm. The behavior of the coercivity of the as-deposited sample as a function of film thickness is typical of most transition metals and their alloys, including all of the CoFeB compositions that we studied. Generally, coercivity initially increases with layer thickness, peaks, and then decays to a constant value.

Upon annealing the sample at $T_a = 450$ °C, an overall increase in the coercivity is observed in comparison to the as-deposited amorphous case. Most remarkably, one observes a sharp and large increase (by a factor of 5) in the coercivity at a film thickness of around 22 nm. After this conspicuous transition, the coercivity is observed to decay as expected, but it remains substantially higher in magnitude as compared to the as-deposited case. Figure 2(b) examines the individual hysteresis loops in the three regions of interest as indicated by the arrows in Fig. 2(a); before $t = 10$ nm (1), after $t = 40$ nm (3), and in the sharp transition region of $t = 22$ nm (2). In Region 1, before the sharp transition, a square hysteresis loop is recorded, which is typical for easy (soft)

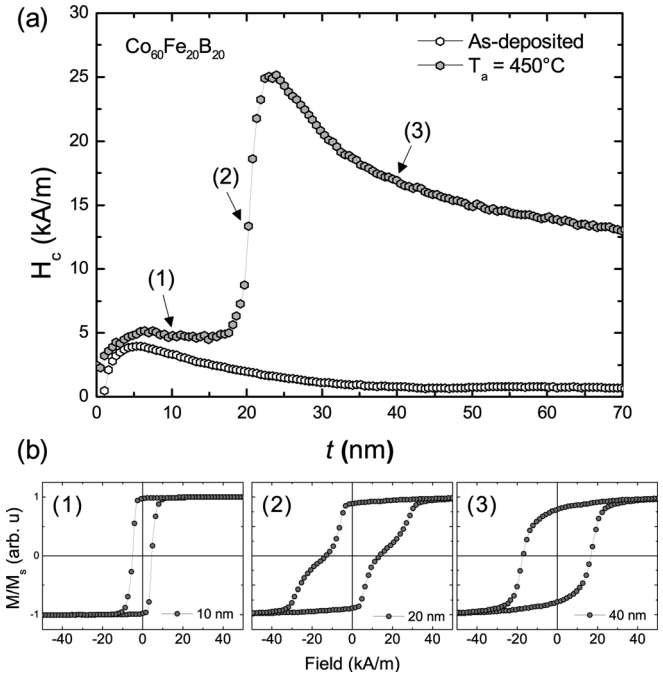


FIG. 2. (a) Coercivity plotted as a function of thickness measured with MOKE for a $Co_{60}Fe_{20}B_{20}$ wedge on an as-deposited and annealed ($T_a = 450$ °C) sample. The arrows indicate the data points at different thicknesses of the $Co_{60}Fe_{20}B_{20}$ wedge for which the MOKE hysteresis loops are shown in (b).

magnetization switching, by either easy domain wall motion or easy domain reversal (domain nucleation). In Region 3, after the sharp transition, a rounded loop is observed, which is typical for (hard) magnetization reversal that is dominated by domain wall pinning at grain boundaries. In Region 2, at the transition, a combination of a square and a rounded loop is seen, indicating that both reversal mechanisms are present at the transition region. Based on previous studies,[12,13,19] it is known that annealing the as-deposited sample crystallizes the CoFeB, which explains the overall increase in coercivity that is observed in Fig. 2(a). However, crystallization alone cannot explain the sharp and large change in coercivity that is observed around $t = 22$ nm, because it is known that layers thinner than 22 nm also crystallize after annealing at $T_a = 450$ °C.[12,13,19]

These observations show that the effect of the crystallization on the magnetic properties of $Co_{60}Fe_{20}B_{20}$ is thickness dependent, suggesting that the local morphology of the layer may have a large effect on the coercivity. A key parameter, then, would be the size of the crystallized grains. The width of the x-ray diffraction peaks can be used to obtain a measure for the out-of-plane grain size $D$ (the coherence length) by using the Paul Scherrer formula $D = 0.89\,\lambda/B\cos(\theta)$. Here, $\lambda$ is the x-ray source wavelength, $B$ is the full width at half maximum of the diffraction peak, and $\theta$ is the diffraction angle. Based on this analysis, the out-of-plane grain size is estimated to be $\approx 23$ nm. Note that this grain size is close to the layer thickness at which the rapid transition in the coercivity is observed in the MOKE loops. This might indicate that the layer thickness has an effect on the grain size where the transition to high coercivity is seen. To further substantiate the key role of morphology and layer thickness, we directly address this using HRTEM in the next section, which then allows a further analysis of the magnetic phenomena in Sec. VI.

## V. HRTEM ANALYSIS

In order to further investigate the role of the morphology and grain growth, we performed HRTEM on lamella prepared from a $Co_{60}Fe_{20}B_{20}$ wedge sample annealed at $T_a = 450$ °C, identical to the sample represented in Fig. 2. Two lamella were prepared from the same sample at $t \approx 10$ nm and 50 nm, respectively, in order to investigate the difference in crystallization before and after the sharp transition region in the magnetic behavior.

Figure 3(a) shows a low magnification bright field HRTEM image of the layer at $t \approx 50$ nm. The dark/white contrast in the layer corresponds to differently oriented crystalline grains. The morphology of the layer seems to consist of three regions, as indicated on the right of Fig. 3(a). Region i denotes the bottom $SiO_2$/Al interface, and Region iii denotes the top CoFeB/Al interface. In both of these regions, randomly oriented *small* grains are observed, whereas in the bulk of the layer, denoted as Region ii, grains with larger sizes are observed. The grains at the $SiO_2$/Al bottom interface extend up to $\approx 12$ nm into the CoFeB layer, whereas the grains at the CoFeB/Al top interface are smaller ($\approx 3$ to 5 nm) and less apparent as compared to those at the $SiO_2$/Al bottom interface.

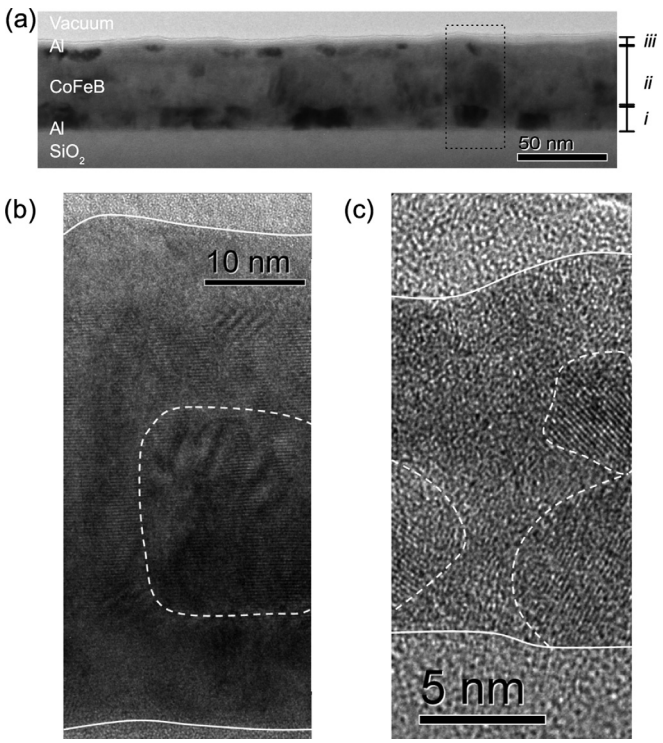


FIG. 3. High-resolution cross-section transmission electron microscopy (HRTEM) images of a $Co_{60}Fe_{20}B_{20}$ sample annealed at $T_a = 450$ °C. (a) Low and (b) high magnification images of the lamella prepared at a layer thickness of $t \approx 50$ nm. A high magnification of the area indicated by the box in (a) is given in (b). The regions indicated by i, ii, and iii are discussed in the text. (c) HRTEM image of lamella prepared at $t \approx 10$ nm. The white lines indicate the interface with the substrate and vacuum; the striped white lines indicate grains (boundaries).

In Fig. 3(b), a high magnification HRTEM image of the layer at $t \approx 50$ nm can be seen for the area indicated by the dotted box in Fig. 3(a). In this image, the morphology of the layer can be seen to consist of two aspects: (1) Relatively large grains with sizes of up to $\approx 20$ nm occupy the bulk of the layer, consistent with the grain sizes derived from the XRD measurements in Fig. 1. One such grain is indicated by the white dashed line in the middle of the layer. (2) Randomly oriented smaller grains can be seen at both the top and the bottom interfaces. Together, these two aspects suggest that the interfaces with the top and bottom Al layers induce a crystallization with small random grain sizes, while the larger grains are allowed to form in the bulk of the layer.

In Fig. 3(c), a HRTEM image of the lamella prepared at $t \approx 10$ nm is shown; some grains are indicated with a white dashed line. The layer is clearly crystallized and contains randomly oriented small grains with a grain size of $\approx 3$ to 5 nm. Both images in Figs. 3(b) and 3(c) suggest that when the layer is thin, the average grain size $D$ remains small. However, when the layer thickness increases above the sum of these interfacial layer grain sizes, large grains can grow in the bulk of the layer, which is less influenced by the interfaces. In other words, one may infer that the film thickness limits the average grain size $D$ as the interfaces induce smaller grains, and as the layer thickness increases, large grains can develop in the bulk of the film. Such a film thickness limited growth behavior has been reported by Takeuchi *et al.*[18] Now that we have direct proof that the layer thickness has a limiting effect on the grain size, let us focus on a model that can relate the grain size to the observed sharp increase of the coercivity in the annealed film as shown in Fig. 2.

## VI. RANDOM ANISOTROPY MODEL

The increase in coercivity, as discussed in Sec. IV, can be explained by the random anisotropy model (RAM), first introduced by Alben *et al.*[15] The RAM suggests that the magnetic behavior changes from soft to hard when the grain size $D$ becomes of the order of the magnetic exchange length $L_{ex}$. When $D < L_{ex}$, an averaging of the magnetic crystalline anisotropy allows easy domain wall motion or domain nucleation, which leads to a low coercivity. This is generally the case in a TM-B based amorphous or nanocrystalline material and results in the soft magnetic behavior. On the other hand, when $D \approx L_{ex}$, the averaging of the magnetic crystalline anisotropy increasingly vanishes, and the crystalline grain boundaries act as strong magnetic domain boundaries. In this case, the magnetization reversal is dominated by the pinning of domain walls at grain boundaries, leading to a higher coercivity.

Recalling the postanneal hysteresis loops shown in Fig. 2(b) (1), we observed a square hysteresis loop typical of easy magnetization switching for films thinner than $t < \approx 18$ nm. From the HRTEM analysis, we concluded that in the case of thin films, the grain sizes are limited by the film thickness, which hinders the growth of grains in the bulk of the film, while the interfacial grains remain small. We found that grains at the bottom interface were $\approx 12$ nm whereas those at the top interface were $\approx 3$ to 5 nm in size, amounting to $\approx 15$ to 17 nm. In accordance with the RAM, one may infer that in this layer thickness regime, $D < L_{ex}$ and an averaging of the magnetic crystalline anisotropy takes place, which leads to a low coercivity.

For films thicker than $t > \approx 23$ nm, the postanneal hysteresis loops shown in Fig. 2(b) (3) showed a rounded hysteresis loop, which is typical of magnetization reversal that is dominated by domain wall pinning at grain boundaries. From the HRTEM analysis, we concluded that in the case of thicker films, larger grains start growing in the bulk of the layer, which allows $D \geq L_{ex}$ so that the averaging of the magnetic crystalline anisotropy is quenched and the crystalline grain boundaries start acting as strong magnetic domain boundaries.

The double loop in Fig. 2(b) (2) can be explained by the coexistence of regions with small and large $D$ compared to $L_{ex}$ in the transition region around $t = 20$ nm. In other words, the double loop is a combination of the low coercivity from the small grains and the high coercivity of the large grains starting to appear at $t = 18$ nm in the bulk of the layer. Now that we can explain the change in the coercivity for one annealing temperature, we will concentrate on the effect of the annealing temperature on the magnetic properties.

## VII. ANNEALING TEMPERATURE

The above analysis is endorsed by probing the coercivity as a function of annealing temperature, which influences the grain size and the degree of crystallinity of the films. Figure 4 shows the coercivity of identical $Co_{60}Fe_{20}B_{20}$ wedges annealed at different temperatures. We observe no change in coercivity between the as-deposited and the $T_a = 375$ °C samples, although broad diffraction peaks appeared in the XRD spectrum at $T_a = 300$ °C. Because the grain sizes derived from the XRD data at such low annealing temperatures were found to be quite small, the insensitivity of the coercivity to annealing at these temperatures clearly suggests that sufficiently large grains are needed to induce an increase in coercivity. In other words, one may conclude that for $T_a < 375$ °C, $D < L_{ex}$.

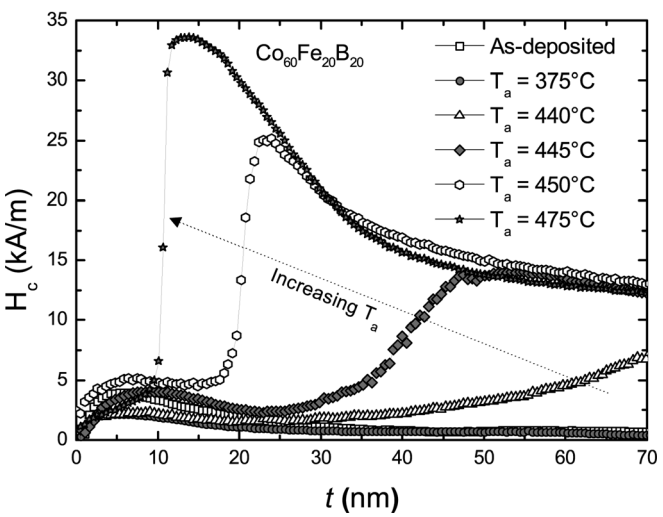


FIG. 4. Coercivity as a function of the thickness of $Co_{60}Fe_{20}B_{20}$ for different annealing temperatures.

The increase in coercivity starts to develop for $T_a > 440$ °C at the thick end of the wedge. For $T_a = 440$ °C and $T_a = 445$ °C, the coercivity increases gradually with the film thickness. For $T_a > 445$ °C, the coercivity shows a progressively sharper transition. This transition from a gradual to an increasingly sharp response of the coercivity for higher $T_a$ can be explained by differences in the spread of the grain sizes. We suggest that for the thick part of the film, grains with a large spread in size begin to grow in the bulk of the film, unimpeded by the interfaces. As $T_a$ increases, the grains grow, and following the RAM (i.e., when $D \rightarrow L_{ex}$), the coercivity increases. Because the grain sizes are limited by the film thickness $t$ and the annealing temperature $T_a$, the film thickness at which $D \rightarrow L_{ex}$ varies.

Coming to the degree of sharpness of the increase in coercivity, from Fig. 4 it is clear that this transition of $H_c$ gets sharper for a thin layer. This can be understood using the RAM, which predicts an increase in $H_c$ with $\sim D^n$, where $n = 3$ to 6, when $D$ approaches $L_{ex}$.[15,21] Recalling the limiting effect of the interfaces, and thus the film thickness, on the grain sizes, we can use the change in $t$ to approximate the increase in $D$. The abrupt increase in $H_c$ seen for $T_a > 450$ °C indeed shows this power law trend, and we have to keep in mind that in the transition region an average grain size should be used.

The change of $H_c$ after the transition is expected to decrease with $1/D$ (domain wall pinning).[21] However, the decrease in $H_c$ that we observe does not scale with $1/t$ (not shown), indicating that $D$ after the transition does not directly scale with $t$ due to multiple grains in the film thickness that have formed in the thicker region.

We can conclude that the observed trends of $H_c$ with the annealing temperature can be explained within the RAM model and thus open up the possibility of tuning $D$ by choosing a suitable layer thickness and annealing temperature. Finally, we turn to the effect of the CoFeB composition on the magnetic properties when annealed; we again relate the observed trends to the RAM.

## VIII. COMPOSITION DEPENDENCE

Figure 5 shows $H_c$ as function of $t$ for different $Co_{80-x}Fe_xB_{20}$ compositions at $T_a = 450$ °C. Note the large difference in scale on the vertical axis between Fig. 5(a) and Fig. 5(b). For low Fe contents, a sharp increase in $H_c$ is seen [Fig. 5(a)], similar to that observed for $Co_{60}Fe_{20}B_{20}$. However, for high Fe contents [Fig. 5(b)], we see that there is no significant change in $H_c$, apart from the increase at low thickness due to the shape anisotropy of the thin film. The reason that the increase in $H_c$ is seen only for low Fe content alloys may be explained by the difference in $L_{ex}$ between Fe and Co. For Fe, Löffer *et al.*[22] obtained $L_{ex,Fe} = 35$ nm, and they estimate $L_{ex,Co} = 16$ nm for Co by directly varying $D$. Although these numbers are reported only for pure Co and Fe, to the first approximation, the ratio of $L_{ex,Fe}/L_{ex,Co} \approx 2$ may be argued to hold for our samples as well. In view of the experimental fact that the grain size approximated for the $Co_{60}Fe_{20}B_{20}$ films from XRD in Fig. 1 and HRTEM in Fig. 3 for $T_a = 450$ °C is $\approx$ 20 nm, this shows that, indeed, $D >$

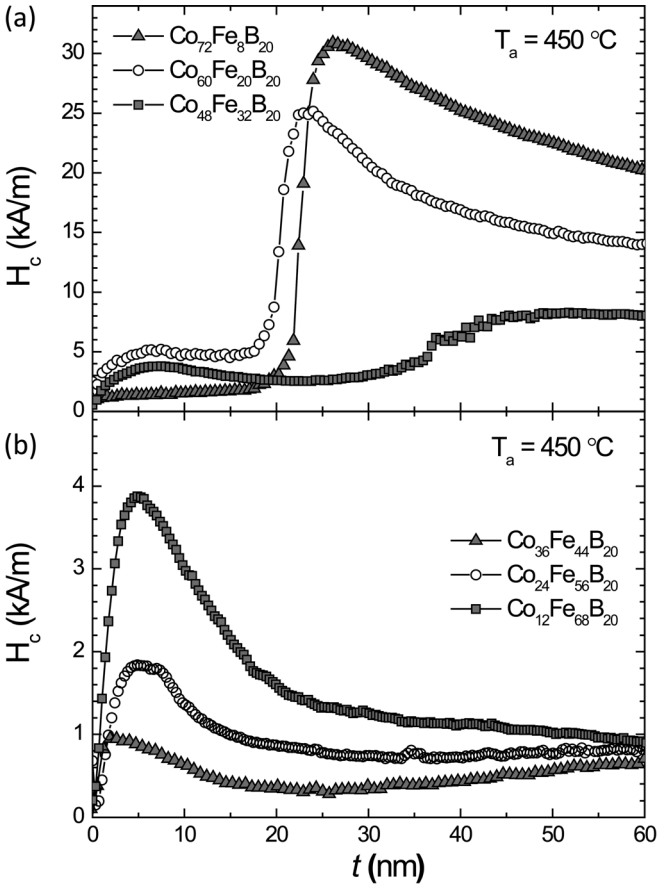


FIG. 5. Coercivity of $Co_{80-x}Fe_xB_{20}$ annealed at 450 °C. (a) $H_c$ for $x = 8\%$, 20%, and 32%. (b) $H_c$ for $x = 44\%$, 56%, and 68%. A sharp increase in $H_c$ is found after annealing for samples with a low iron content. Note the large difference in scale on the $y$-axis between (a) and (b).

$L_{ex,Co}$, and indicates that this can induce the transition to the higher coercivity for Co rich samples. Moreover, from the XRD performed on all of the compositions (not shown), we cannot identify a large difference in $D$ between Fe rich and Co rich CoFeB compositions within the accuracy of the technique. This leads us to suggest that the difference in $L_{ex}$ between Co rich and Fe rich $Co_{80-x}Fe_xB_{20}$ is responsible for the observed transition to a high $H_c$ in low Fe content compositions.

The fact that the thin parts of the films do not show an increase in $H_c$ for commonly used $T_a$ hints at why the ternary CoFeB alloys are so interesting for applications. The thin crystalline films (< 20 nm) used in TMR and spin torque applications ensure that $D$ will remain below $L_{ex}$, and thereby the soft magnetic properties critical for the sharp magnetization switching needed in devices will be retained.

## IX. CONCLUSION AND FINAL REMARKS

In summary, we show that $Co_{80-x}Fe_xB_{20}$ alloys can be crystallized by annealing. This opens up the possibility of tuning the grain size in the CoFeB films by choosing the films thickness and $T_a$. Finally, we relate the transition from soft to hard magnetic properties to an interplay between the magnetic exchange length and the crystallite grain size. This allows us to explain the observed trends in $H_c$ as a function

of thickness and composition. Thus, keeping the thickness of the $Co_{80-x}Fe_xB_{20}$ films below 20 nm ensures that the grain size will remain below $L_{ex}$ and that the films will thereby keep the soft magnetic properties critical for the sharp magnetization switching needed in devices.

## ACKNOWLEDGMENTS

This work was supported by NanoNed, a Dutch nanotechnology program of the Ministry of Economic Affairs. The authors acknowledge financial support from the European Union under the Framework 6 program under a contract for an Integrated Infrastructure Initiative. Reference 026019 ESTEEM.

[1]K. Moorjani and J. M. D. Coey, Metallic Glasses (Elsevier, Amsterdam, 1984).
[2]D. Wang, C. Nordman, D. M. Daughton, Z. Qian, and J. Fink, IEEE Trans. Magn. **40**, 2269 (2004).
[3]D. D. Djayaprawira, K. Tsunekawa, M. Nagai, H. Maehara, S. Yamagata, N. Watanabe, S. Yuasa, Y. Suzuki, and K. Ando, Appl. Phys. Lett. **86**, 092502 (2005).
[4]K. Tsunekawa, D. D. Djayaprawira, M. Nagai, H. Maehara, S. Yamagata, N. Watanabe, S. Yuasa, Y. Suzuki, and K. Ando, Appl. Phys. Lett. **87**, 072503 (2005).
[5]J. Hayakawa, S. Ikeda, F. Matsukura, H. Takahashi, and H. Ohno, Jpn. J. Appl. Phys. **44**, L587 (2005).
[6]A. A. Tulapurkar, Y. Suzuki, A. Fukushima, H. Kubota, H. Maehara, K. Tsunekawa, D. D. Djayaprawira, N. Watanabe, and S. Yuasa, Nature **438**, 339 (2005).
[7]S. Ikeda, K. Miura, H. Yamamoto, K. Mizunuma, H. D. Gan, M. Endo, S. Kanai, J. Hayakawa, F. Matsukura, and H. Ohno, Nature Mater. **9**, 721 (2010).
[8]J. Hayakawa, S. Ikeda, Y. M. Lee, R. Sasaki, T. Meguro, F. Matsukura, H. Takahashi, and H. Ohno, Jpn. J. Appl. Phys. **44**, L1267 (2005).
[9]H. Kubota, A. Fukushima, K. Yakushiji, T. Nagahama, A. Fukushima, S. Yuasa, K. Ando, H. Maehara, Y. Nagamine, K. Tsunekawa, D. D. Djayaprawira, N. Watanabe, and Y. Suzuki, Nat. Phys. **4**, 37 (2008).
[10]D. Kirk, A. Kohn, K. B. Borisenko, C. Lang, J. Schmalhorst, G. Reiss, and D. J. H. Cockayne, Phys. Rev. B **79**, 014203 (2009).
[11]P. V. Paluskar, R. Lavrijsen, M. Sicot, J. T. Kohlhepp, H. J. M. Swagten, and B. Koopmans, Phys. Rev. Lett. **102**, 016602 (2009).
[12]Y. M. Lee, J. Hayakawa, S. Ikeda, F. Matsukura, and H. Ohno, Appl. Phys. Lett. **90**, 212507 (2007).
[13]K. Tsunekawa, Y. S. Choi, Y. Nagamine, D. D. Djayaprawira, T. Takeuchi, and Y. Kitamoto, Appl. Phys. Lett. **87**, 072503 (2005).
[14]G. I. R. Anderson, H.-X. Wei, N. A. Porter, D. A. Arena, J. Dvorak, X.-F. Han, and C. H. Marrows, J. Magn. Magn. Mater. **322**, 756 (2010).
[15]R. Alben, J. J. Becker, and M. C. Chi, Appl. Phys. Lett. **49**, 1653 (1978).
[16]S. Cardoso, C. Cavaco, R. Ferreira, L. Pereira, M. Rickart, P. P. Freitas, N. Franco, J. Gouveia, and N. P. Barradas, J. Appl. Phys. **97**, 10C916 (2005).
[17]F. F. Li, R. Shariff, L. X. Jiang, X. Q. Zhang, X. F. Han, Y. Wang, and Z. Zhang, J. Appl. Phys. **98**,113710 (2005).
[18]T. Takeuchi, K. Tsunekawa, Y. S. Choi, Y. Nagamine, D. D. Djayaprawira, A. Genseki, Y. Hoshi, and Y. Kitamoto, Jpn. J. Appl. Phys. **46**, L623 (2007).
[19]P. V. Paluskar, J. J. Attema, G. A. de Wijs, S. Fiddy, E. Snoeck, J. T. Kohlhepp, H. J. M. Swagten, R. A. de Groot, and B. Koopmans, Phys. Rev. Lett. **100**, 057205 (2008).
[20]W. C. Ellis and E. S. Greiner, Trans. Am. Soc. Met. **29**, 415 (1941) (see Fig. 4).
[21]G. Herzer, IEEE Trans. Magn. **26**, 1397 (1990).
[22]J. F. Löffer, H. B. Braun, W. Wagner, G. Kostorz, and A. Wiedenmann, Mater. Sci. Eng., A **304–306**, 1050 (2001).